Production of high quality electron bunches by dephasing and beam loading in channeled and unchanneled laser plasma accelerators[*]

C.G.R. Geddes,[1,†] Cs. Tóth,[1] J. van Tilborg,[1,‡] E. Esarey,[1] C.B. Schroeder,[1] D. Bruhwiler,[2] C. Nieter,[2] J. Cary,[2,§] and W.P. Leemans[1,¶]

[1]*Lawrence Berkeley National Laboratory,*

1 Cyclotron Rd, Berkeley CA 94720

[2]*Tech-X Corporation, 5621 Arapahoe Ave Ste. A, Boulder CO 80303*

(Dated: February 11, 2005)

Abstract

High quality electron beams, with a few 10^9 electrons within a few percent of the same energy above 80 MeV, were produced in a laser wakefield accelerator by matching the acceleration length to the length over which electrons were accelerated and outran (dephased from) the wake. A plasma channel guided the drive laser over long distances, resulting in production of the high energy, high quality beams. Unchanneled experiments varying the length of the target plasma indicated that the high quality bunches are produced near the dephasing length, and demonstrated that channel guiding was more stable and efficient than relativistic self-guiding. Consistent with this data, particle in cell simulations indicate production of high quality electron beams when trapping of an initial bunch of electrons suppresses further injection by loading the wake. The injected electron bunch is then compressed in energy by dephasing, when the front of the bunch begins to decelerate while the tail is still accelerated.

PACS numbers: Valid PACS appear here

I. INTRODUCTION

Laser driven plasma wakefield accelerators have demonstrated high accelerating gradients of up to several hundred GV/m[1–7], making them attractive as next generation sources of particles and radiation[8,9]. The ponderomotive or radiation pressure of an intense laser pulse is used to drive a density oscillation (wake) in a plasma, the longitudinal field of which accelerates particles[8]. Historically, electron beams produced had 100% energy spread[1–7], limiting applications. Recently however, experiments have produced beams of narrow energy spread by extending the distance of propagation using a guiding channel[10]. Similar beams have also been observed using a large laser spot size to increase the diffraction range $Z_R = \pi w_0^2 / \lambda$ with w_0 the spot size, and hence the propagation distance of the laser pulse through the gas jet[11,12]. Understanding and optimizing the physics responsible for producing these narrow energy spread beams is important to allow development of laser accelerators for radiation sources[13–15], high energy physics[16], and other applications requiring small energy spread and stable beams.

Due to the periodic structure of the accelerating field of the wake, electrons injected at different phases (longitudinal positions behind the laser pulse) experience different accelerating fields, leading to large energy spread. While phase controlled optical injection techniques[17–21] have been proposed in order to reduce energy spread, these have not yet been fully demonstrated experimentally. Rather, current experiments, including those described above, use relatively high density plasmas, where the laser pulse is modulated to match the plasma period by the nonlinear response of the plasma (self modulation[22]) and very high amplitude wakes are excited. When the wake reaches the so called wave breaking amplitude, electrons are trapped from the bulk plasma and accelerated[1,5–7]. The group velocity of the laser and hence the phase velocity of the plasma wave is lower at high density, reducing the wave breaking threshold and allowing trapping of electrons at accessible laser intensities. Self-trapping such as this can inject particles over a wide phase range leading to the expectation that such accelerators would not produce beams of narrow energy spread, an expectation which was borne out by experiments until recently.

Here we present experiments, carried out at the L'OASIS facility of Lawrence Berkeley National Laboratory (LBNL), and simulations, with the code VORPAL[23], which show that high quality electron bunches were formed in the self trapped, self modulated regime by a

combination of beam loading and dephasing. We find that electron bunches of narrow energy spread and high energy are preferentially produced when the accelerator length matches the dephasing length L_{deph} over which the electrons outrun the wake and slip into decelerating phase.

Section II describes channeled wakefield acceleration experiments, which produced the highest quality electron bunches observed, by guiding the drive laser pulse using a plasma density channel to produce a long, controlled interaction length. Section III describes particle in cell simulations consistent with these experiments which indicate that beam loading, where the accelerated electrons alter the wake, allows the formation of the low energy spread bunch by turning off injection after the self trapping of the initial group of electrons, effectively creating a self consistent phased electron load. At the dephasing length, these particles are concentrated in energy because of their rotation in phase space, forming the narrow energy spread bunch. Section IV describes unchanneled experiments where plasma lengths less than, equal to, and greater than the dephasing length were used. Bunches with low energy spread were produced by matching the plasma length to the dephasing length, but these beams were less stable and produced less charge than channeled experiments at the same power. Section V summarizes the results and offers applications and opportunities for further development.

II.   CHANNELED WAKEFIELD ACCELERATION EXPERIMENTS

A pre-formed plasma density channel was used to extend and control the focused propagation distance of the drive laser pulse in the plasma. The channel was created in a gas target by two laser pulses using a variant of the ignitor-heater method[24], with the multi-arm L'OASIS Ti:Sapphire laser[25,26]. The laser operates at 800 nm with chirped pulse amplification[27], providing up to 10 TW of laser power in a drive beam as well as secondary beams for channel formation and injection. For these experiments, a nearly uniform 2.4 mm long gas target at an atomic density near 4×10^{19} cm^{-3} was provided by a supersonic hydrogen gas jet. A 60 fs, 15 mJ ignitor pulse was focused at f/15 near the downstream edge of the gas jet. The focal location and f/number were chosen so that beam convergence roughly balanced ionization induced refraction[28,29], producing a cylindrical plasma of nearly uniform radius. This plasma was subsequently heated to tens of eV by inverse Bremsstrahlung using ~ 50

mJ from a 250 ps, 150 mJ pulse cylindrically focused and incident on the jet from the side. This arrangement is shown in Fig. 1. Use of two channel formation pulses allowed both efficient ionization (requiring a high intensity pulse) and heating (optimized with a longer, low intensity pulse)[24]. The resulting hot plasma filament on axis expanded outward, driving a shock wave in the surrounding neutral gas. This shock resulted in a density depletion on axis and a nearly parabolic transverse density profile[30]. Solution of the wave equation shows that such a profile can be matched to guide a gaussian laser pulse without distortion in the low intensity limit where relativistic effects are not important. For a density rise of $\delta n = 1/\pi r_e r_s^2$, over a spot size r_s and where r_e is the classical electron radius, the change in phase velocity induced by rising density just counters diffraction, and the laser pulse remains collimated. Guiding at intensities up to 2×10^{17} W/cm^2, which are too low to trap and accelerate electrons, has been demonstrated by previous experiments using this method[24,31–34].

A. Guiding of Relativistically Intense Laser Pulses in Plasma Channels

Guiding at high intensity, as desired for wakefield acceleration, requires controlling both diffraction and relativistic modification of the plasma refractive index[35]. Relativistic self-guiding occurs when the laser is intense enough that the quiver motion of the electrons causes their mass to increase, changing the refractive index[36–39]. This effect, which occurs in regimes of interest to wakefield acceleration, provides some self-guiding for laser powers above the critical power P_c, but is unstable, eventually destroying the pulse and limiting propagation distance[35,40,41]. In the present experiments, the drive pulse is of relativistic intensity, and so the channel profile was detuned from the low power matching condition, with a smaller rise in density to compensate for the presence of self-guiding.

The density profile of the channel has been matched to guide the drive pulse by choosing the plasma temperature (which determines shock velocity) using the heater beam, and by adjusting the timing of the guide pulses. The drive pulse, which was collinear with the ignitor and focused near the entrance of the channel, had a 55 fs pulsewidth full width at half maximum (FWHM), with powers of 0-9 TW and a focused spot size of 7 to 8.5 μm. To tune the channel, the plasma and its evolution were characterized interferometrically using a frequency doubled (405 nm wavelength) pulse incident from the side, with fs temporal

resolution. An imaging system using cylindrical optics provided spatial resolution of 17 μm × 4 μm, to allow viewing of the long narrow plasma channels. The phase map from the interferometer was Abel inverted to recover the electron density assuming a cylindrically symmetric distribution. Symmetry is confirmed by the round mode structure of the guided laser pulse (below).

Drive pulses below the self-guiding threshold were well guided by channels with radial density profiles tuned to match the low power guiding condition described above. As power was increased above the self-guiding threshold, the output mode distorted in such matched channels, and the channel was adjusted to compensate for the presence of self-guiding by reducing the radial density gradient. Guiding of drive pulses up to 4 TW ($2P_c$) has been obtained without aberration of the laser mode and without self trapping of electrons[42]. This provides a long scale length structure for experiments on controlled injection which may stabilize and increase quality of beams from laser accelerators[17,18,21]. Above 4 TW the beam is still well guided, but some distortion of the laser mode was always present (see below) due to the strong contribution of self-guiding.

Optimal guiding of the drive pulse at 9TW, and optimal acceleration of self trapped electron bunches, was observed in channels having an axial density of $1.9 \times 10^{19} \text{cm}^{-3} \pm 10\%$ over the central 1.7 mm of the jet. The length of the wake drive laser pulse was thus longer than the linear plasma period, providing operation in the self-modulated regime[22,38]. This allowed the channels to extend laser propagation distance and enhance acceleration performance in self modulated wakefield accelerators, where high densities allow self trapping and acceleration of electrons[10,43]. The profile of the channel, shown in Fig. 2, had a $\sim 40\%$ reduced rise in density over a laser spot size compared to the matched profile for a low intensity pulse[24]. This detuning was required to optimize guiding of the 9 TW pulse, due to the contribution of self-guiding for this power.

The plasma channel guided the drive pulse, maintaining its intensity and nearly eliminating diffraction over 10 Z_R, as shown in Fig. 3. After the propagation of the 9 TW drive pulse, the side interferometer image (Fig. 3A) showed a plasma only slightly wider than the original channel diameter (Fig. 2A). This indicates that the drive pulse was well confined within the channel since leakage of the drive pulse from the channel ionizes the surrounding neutral gas. The spatial mode of the laser pulse was characterized using a mode imaging camera, which could be translated to image the input or output of the channel. This mode

image (Fig. 3B) showed an intense spot of 24 μm FWHM containing 10% of the input energy, confirming that the drive pulse was well guided. The spot is circular, confirming that the guiding channel is cylindrically symmetric. The reduction by a factor of 10 in energy from the input spot is due to a combination of leakage from the channel and depletion of the laser energy to excite the wakefield. Enlargement of the spot compared to the 8.5 μm input and the leakage outside the guide appeared as the input intensity was increased beyond two times the relativistic self focusing threshold. This is believed to be due to the inability of the channel to perfectly control the spot size in the presence of intense self-guiding. The enlargement due to this effect is small however compared to the diffraction displayed when the channel is off. In this case, the interferometer (Fig. 3C) showed a plasma which expands rapidly in the propagation direction, indicating that the laser is diffracting. The laser mode image (Fig. 3D) showed a diffuse transmitted spot with a diameter near 100 μm. Correlation of the mode imager and interferometer measurements showed that an intense guided mode was present only when the interferometer indicated that the laser was well confined to the channel. We next describe the effect of using a preformed plasma channel on the electron acceleration process.

B. Electron Acceleration in Plasma Channels

Electrons trapped and accelerated by the plasma wave were momentum dispersed using a magnetic spectrometer with a bend angle of 55° to obtain the electron energy spectrum. The electron beam was then detected by a phosphor screen imaged onto a charge coupled device (CCD) camera (see Fig. 1). The energy range covered in a single shot was ±15% about a central energy selectable from 0-80 MeV, allowing structure in the energy distribution to be observed on a single shot basis. A full spectrum from 0-92 MeV averaged over many shots was obtained by scanning the magnet current. The multi-shot spectrum allowed determination of the peak energy achieved and shot-to-shot statistics at a given energy. A slit was used at the input of the spectrometer to give ±2% energy resolution. To detect electrons above 92 MeV, a separate phosphor observing bend angles of 0-5° was used. Because of the small bend angle and observation down to 0°, this diagnostic could observe electrons of arbitrarily high energy, but could not resolve the energy spread of the beam. In either configuration, the beam divergence was obtained in the undispersed direction. The magnetic

6

spectrometer was calibrated against an integrating charge transformer, located before the slit and subtending f/8, to obtain the charge in the electron beam. To measure the spatial shape of the electron beam, and to provide a divergence measurement integrated over all energies, a beam phosphor screen (BPS) could be inserted prior to the magnet, showing the spatial profile of the energy integrated beam.

The magnetic spectrometer showed that the channel guided accelerator produced electron bunches with a large fraction of the charge in a well defined bunch at 86 MeV with 3.6 MeV energy spread FWHM and 3 mrad divergence FWHM (Fig. 4), in contrast to previous experiments which observed beams of continuous energy spread. The BPS confirmed that the channel guided accelerator (Fig. 5A) produces collimated beams, with divergence near 6 mrad FWHM (integrated over all energies). The beam is nearly circular, so that the 1-dimensional divergence measurement from the spectrometer is representative, and the divergence of the bunch at 86 MeV (Fig. 4) was half that of the integrated beam observed on the BPS, consistent with previous experiments that have shown that higher energy electrons were more collimated[6]. The energy spread of the peak, at $\pm 2\%$, is essentially limited by the spectrometer resolution so that the beam may in fact have narrower energy spread. The peak at 86 MeV shows a contrast ratio greater than 10:1 above a broad distribution of charge extending on either side. To determine the charge of this high energy bunch, the spectrometer current was scanned to obtain a full spectrum from 1 to 90 MeV averaged over 300 shots. The integral of this average spectrum was calibrated to the integrating charge transformer (ICT), accounting for the beam size and for the average overlap of the beam with the spectrometer slit as observed on the BPS. This calibration was verified by changing the slit size and observing that the amplitude of the spectrum changed by the expected ratio. The calibration of the magnetic spectrometer has also been verified by nuclear activation measurements. This provides a lower limit on the charge in the 86 MeV beam of 2×10^9 electrons, assuming 100% transmission through the slit.

To obtain an estimate for the emittance it is first noted that space charge effects should be minimal for this relativistic beam. Assuming ballistic propagation from a source the size of the laser spot in the channel ($\sim 8.5\ \mu$m at entrance, $\sim 24\ \mu$m at end) is then a reasonable first approximation. The 3 mrad divergence of the high energy beam then indicates a geometric RMS emittance ϵ_x of 0.005-0.01 π mm-mrad and a normalized emittance of 1-2 π mm-mrad RMS, comparable to the best state of the art rf facilities[16]. The above represents an upper

7

limit, as it is likely the electron beam comes from a source smaller than the initial laser spot size (simulations, below, indicate a source size near $4\mu m$) indicating that a normalized emittance as small as 0.5 π mm-mrad is possible.

The quality of optical guiding as well as the pointing, quality and charge of the electron beams at high energy fluctuated from shot-to-shot, probably caused by laser pointing jitter that changes the overlap between the wake drive pulse and the channel formation pulses (and hence guide quality and incoupling) as well as laser power fluctuations. Beams with 3×10^9 electrons have been observed at similar energies (78 ± 3 MeV FWHM), and electrons were observed up to the limit of our 55° high-resolution spectrometer (92 MeV). Using the 5° spectrometer, we observed bunches at energies of 150 MeV, but this diagnostic did not allow the fine resolution required to resolve energy spread. Structure in the energy spectrum has been seen for electrons with energy as low as 15 MeV. Below 15 MeV there was an essentially continuous distribution, and total beam charge was 1.7×10^{10} electrons as measured by the ICT, subtending f/8. Using a bend magnet, the low-energy contribution can be separated, leaving a high-energy, high-quality beam with a few times 10^9 electrons. Consistent control of guiding and electron injection[17–21] in order to stabilize these beams are among the next challenges for laser accelerators.

C. Correlations between accelerated electron yield and laser beam properties

Well guided optical beams were highly correlated with the acceleration of electrons to high energies. Simultaneous observation of the mode image and the 5° spectrometer over 300 shots allowed measurement of the correlation between guided mode intensity and charge of the electron beam at high energy. Figure 6 shows the charge at energy greater than 100 MeV as a function of normalized guided mode intensity. Normalized guided mode intensity is defined as the peak intensity in the mode image on a given shot normalized to the peak observed on any shot in the run, and parameterizes the effectiveness of the guide in maintaining drive amplitude. Charge is measured by integrating the signal on the phosphor screen, normalized to the maximum charge observed. Data have been binned by guided mode intensity in order to display the dependency. There is a stronger than linear rise of charge with intensity, indicating that good mode transport was very important to high energy electron production, or alternatively, that maintaining drive intensity over long

8

distance is an essential criterion for obtaining high energy electrons. This also is suggestive of the importance of matching the pump depletion distance to the dephasing distance to maximize the accelerator efficiency, though a detailed study of that issue is beyond the scope of the present paper.

We have also studied the correlation between the laser spectrum at the exit of the plasma channels and the generation of high energy electron beams. To analyze the transmitted laser spectra, we divided each measured spectrum into an unshifted (within the laser bandwidth) region, and red shifted and blue shifted bands. The correlation of transmitted energy to high energy electrons was positive, and the correlation was more than twice as strong for red shift as blue shift. Normalizing to spectrally integrated transmission, shots with high charge above 100 MeV had 6% more energy in the spectral lobe red shifted from the fundamental, and 5% less blue shifted energy. Hence, in contrast to previous reports[6], here we observe that the largest plasma waves (indicated by accelerated electrons) were most strongly correlated with red shifting of the laser light. This observation is consistent with fluid simulations and with energy conservation, which indicate that the laser must red shift as it deposits energy in the plasma wave.

To differentiate the effects of channeling from pre-ionization, the ignitor pulse was fired 20 or 80 ps before the drive pulse, pre-ionizing a plasma 80 μm in diameter. The plasma did not expand significantly over 80 ps. Hence there was no shock wave and the transverse density profile was flat at 4×10^{19} cm^{-3} and had no guiding properties. We observed no substantial difference between the drive pulse only (unchanneled, below) and pre-ionized cases in laser propagation, electron yield, or energy spectrum. This indicates that channeling and not pre-ionization was responsible for differences in the electron beams described above, and is also consistent with the expectation that the plasma in the single beam experiment is ionized so early in the pulse that the bulk of the pulse (more than 99.9%) sees an ionized target and is not significantly affected by ionization physics.

III.   SIMULATIONS OF BUNCH FORMATION

Two dimensional particle-in-cell (PIC) simulations using the code VORPAL[23] were conducted to evaluate mechanisms of beam formation and to compare to the structure of the experimental electron spectra. Simulations were performed for the experimental densities

and laser parameters, and analyzed as a function of propagation distance. The simulations used a moving window copropagating with the laser pulse, 90 μm long in the longitudinal direction by 80 μm transversely. The grid was 2700×600 cells with 10 particles per cell. Plasma was loaded over the central 60 μm of the box transversely. The laser is polarized out of the plane of the simulation.

The simulated laser envelope and particle phase space as a function of propagation distance are shown in Fig. 7 , and the wake density is shown in Fig. 8, for the parameters of the channeled experiment. The laser initially enters the plasma with a pulse duration longer than the linear plasma period, and as a result does not excite a large wake or accelerate electrons (Fig. 7A). As it propagates, the laser self modulates to the plasma period. This excites a wake[9] of increased amplitude which can trap and accelerate electrons. Trapping and acceleration of a high energy high quality beam was observed in the first plasma period of the wake (i.e., bucket) behind the laser, with electrons trapped when the laser has propagated $\approx$ 1mm (Fig. 7B). The field of the initial trapped electrons interfered with the wake driven by the laser, reducing its amplitude (beam loading)[44]. This effect can be seen in the reduction of wake amplitude from Fig. 8A (before trapping) to Fig. 8B (after trapping). Further trapping was suppressed by this loading. The initial electrons were then isolated in phase space and able to form a high quality bunch if suitably compressed in momentum space.

The electrons are compressed in momentum to form a high quality beam at the dephasing length[9], the length at which the electrons outrun the wake and slip forward into a decelerating phase. As the leading edge of the bunch dephases and is decelerated, while the trailing edge is still accelerated, the particles are concentrated at the dephasing energy, which is also the maximum energy gain obtainable for the given parameters. In the simulation this results in the formation of a low energy spread bunch after 1.5 mm propagation (Fig. 7c). This optimum length is close to the 1.7 mm length of the high density plateau in the experimental plasma. Electron energy spread increases again with further propagation as the particles are decelerated, unless the plasma is terminated at this point. Peak electron energy remains nearly constant as the particles are mixed to fill all phases in the wake, but the number of electrons at high energy is reduced after 2 mm propagation (Fig. 7d). The bunch dissipates more slowly than it forms since the laser pulse is depleting its energy into the wake as it propagates, resulting in reduced wake amplitude and slower deceleration, and

monoenergetic features are present from $\sim$ 1.3 to 1.9 mm, with the energy of the peak varying from 80 to 220 MeV. The asymmetry may be even greater in three dimensions, where filamentation and other instabilities may further disperse the laser, leading to observation of low energy spread well beyond the dephasing length. Hence we expect that for plasmas shorter than the dephasing length low energy beams with continuous distributions would be observed, while at the dephasing length higher energies and structure (i.e. spikes of narrow energy spread) in the distribution would be present. After the dephasing limit, peak energy should not increase, and structure in the distribution and density of particles at high energy should be reduced. The peak energy observed in these simulations, 220 MeV, is close to the 150 MeV observed in the experiments, and energy spread is likewise percent level in both cases. The simulations show less trapped charge than the experiments by a factor of 10, and comparison with other simulations suggests that this is due to a combination of resolution (trapped charge increased with longitudinal and particle resolution) and 3d effects. Simulations with the laser polarized in the plane of the simulation have shown trapping of 10^9 electrons (though with broader energy spread) under similar conditions, and this has also been observed in 3 dimensional simulations[45].

Wake buckets behind the first one also trap particles, but these do not contribute to the highest energy beam. The difference may be due to transverse wave breaking and laser envelope effects. Due to the nonlinear variation of the plasma wave period with amplitude, the wake phase fronts curve, and curvature increases with increasing distance behind the laser pulse. This curvature reduces the threshold for trapping through transverse wave breaking for buckets far behind the pulse[46]. The trapping threshold has also recently been shown to increase for buckets within the laser envelope (i.e., the first bucket)[47]. Consistent with this, simulations indicate that in buckets far behind the laser pulse the wave breaks and picks up particles early and at low wave amplitude. The peak energy obtainable from the wakefield rises with wave amplitude[9], so these particles dephase early and at low energy, and do not contribute to the highest energy beam. However, as each bucket dephases, its electrons are bunched in at the dephasing energy for that bucket. These energies range from 13-100 MeV, compatible with the observation of structure in the experimental energy spectrum at lower energies. Such structure may result when fluctuations in guide quality terminate the wake early, near the dephasing of a particular bucket, or due to fluctuation in laser and plasma parameters. Other simulations have also observed the formation of

structure in the energy distribution over long propagation distances[48–50].

IV. DEPHASING EXPERIMENTS

The dependence of electron bunch energy and energy spread on dephasing was studied experimentally by changing the length and density of the plasma target. Use of various target conditions allowed evaluation of accelerator performance for accelerator lengths greater than, equal to, and less than the dephasing length. The laser was focused to an intensity of 1.1×10^{19} W/cm^2 in a spot of 8.5 μm FWHM in hydrogen gas jets. The pulse length was 55 fs, a few times the linear plasma period for the densities used, in the self modulated regime[22;38]. As the laser entered the gas, its front edge ionized a plasma. As it propagated, the pulse modulated into sub pulses at the plasma period, trapping particles and accelerating them as described above[1,7,35]. Channeling was not used for these studies, so that they also provide a comparison between channeled and unchanneled operation. To allow evaluation of the electron beam statistics, no slit was used in the magnetic spectrometer, which ensured that most electron beams are captured by the spectrometer acceptance. Momentum resolution is reduced, but bunching in the energy spectrum is still visible.

Variation of gas jet density was accomplished by variation of the backing pressure, while length was varied by using shaped nozzles. The jets were supersonic to produce short edge gradients and a plateau region of nearly constant density whose length was determined by the nozzle size . We used a slit gas jet which provided a plateau of 600 μm or 4 mm long depending on rotation with respect to the laser axis. For intermediate length, a cylindrical jet with a 1.8 mm plateau was used. Operating height of the laser above the jets was $0.5 - 1$ mm, selected to avoid burning the jet with the laser, and was greatest for the longer jets to allow for laser divergence. These selections gave us plasmas 0.6 or 1.8 mm long at 4×10^{19} cm^{-3}, and 0.6 or 4 mm long at 2×10^{19} cm^{-3}. Only the lower density was possible in the 4 mm long plasma, because the greater operating height required for the long plasma allowed the gas to expand further.

Using these variations of jet length and density, acceleration experiments were conducted with plasma length greater, equal to, or less than the dephasing length. Dephasing length was evaluated using simulations, since the experiments were in the self modulated regime in order to allow electron trapping from the background plasma. In this regime, the analytic

solution for the linear dephasing length, $L_d = \lambda_p^3/\lambda^2$ where λ_p is the plasma wavelength[9,51], is not adequate because of the need to account for modulation and trapping. The simulations described above were repeated without guiding for plasma densities of 2 and 4×10^{19}cm^{-3}. The results are qualitatively similar to those described above. Self modulation and dephasing are faster at higher densities, so that the dephasing length decreases and the peak energies drop. Self modulation also occurs more quickly without channeling, as the focusing effect of the channel suppresses radial modulation. At 2×10^{19} cm^{-3}, dephasing length is 1200 μm. At 4×10^{19} cm^{-3}, dephasing length drops further to 600 μm. Hence at 4×10^{19}cm^{-3} lengths of 0.6 mm $\approx L_{deph}$ and 1.8 mm $> L_{deph}$ were available, allowing comparison of beams at and after dephasing. Using the second density of 2×10^{19}cm^{-3}, and lengths of 0.6 mm $< L_{deph}$ and 4 mm $> L_{deph}$ allowed additional comparison of pre and post dephasing beams. Data from the two densities together characterized the nature of the beam before, at, and after dephasing.

The electron energy spectrum of the accelerator operated at a plasma density of 4×10^{19}cm^{-3} is shown in Fig. 9, for plasma lengths of 0.6 mm and 1.8 mm. The 1.8 mm plasma corresponds to the same gas jet conditions as in the channeled experiment. In contrast to the guided accelerator, there is little structure in the electron energy distribution, and the peak energy is lower - below 40 MeV. The divergence of the beam is also much broader, near 50 mrad, as shown in Fig 5B. The peak energies observed in the averaged spectrum are similar at both plasma lengths, indicating that no acceleration occurred beyond 0.6 mm. Individual phosphor images (Fig 9 inset),show that there is substantially more structuring of the spectrum in the short plasma. Both features are consistent with a dephasing length near 600 μm at this density, which is also close to the 600 μm dephasing length seen in simulations. Beyond that length there should be little energy gain, and monoenergetic features should be washed out, as observed.

With a plasma density of 2×10^{19}cm^{-3} the character of the energy spectra changed (Fig. 10), consistent with the increased dephasing length at the lower density. The averaged experimental energy spectrum for a plasma length of 0.6 mm shows low peak energies, while the individual phosphor images (inset) show no structure in the distribution. This is consistent with the electron beam being extracted well before dephasing. In contrast, the averaged spectrum at 4 mm plasma length shows that high energies are produced. Individual images show the appearance of monoenergetic structures in the spectrum at high energy.

These features indicate the beam is extracted at or after dephasing. This data is also consistent with the dephasing length of 1200 μm observed in simulations at this density.

The scaling of peak energy observed with density is roughly consistent with the theoretical scaling of maximum energy gain at dephasing. At dephasing, energy gain is proportional to the reciprocal of plasma density for constant E_{max}/E_0, where E_{max} is the maximum accelerating field and E_0 is the wave breaking field[9]. The peak energy observed at 2×10^{19} cm^{-3} was above 90 MeV at 4 mm propagation distance, compared to 40 MeV at 4×10^{19} cm^{-3}. The same scaling of energies is observed in the simulations, which also show that E_{max}/E_0 is the same for the two cases. The peak energies observed are roughly 60% of those obtained in simulations, possibly because the two dimensional simulations do not model well instabilities such as filamentation that can disrupt the drive beam. The phosphor screen used in the spectrometer also has a high detection threshold of a few 10^7, which limits detection.

Charge and energy of the beams fluctuated significantly in the unchanneled accelerator using the low density plasma. This may be due to instabilities in relativistic self-guiding[35], which was used to guide the laser pulse over the several mm (≈ 10 diffraction ranges) required to achieve the dephasing condition in this case. Analysis of the laser mode transmitted through the plasma was performed using the mode imager camera. This showed that the transmitted laser profile was in fact highly unstable, as expected, often breaking into many beamlets. The instability of the beam may in fact be partly responsible for the production of high energy beams in the long plasma; even if the plasma is longer than the dephasing length, drive beam breakup and depletion may have stopped acceleration near dephasing on some shots. Hence, while the single beam experiment demonstrates the dephasing physics, in order to obtain stable beams at high energy use of a guiding channel will be important in order to obtain stable propagation.

Comparing the single beam experiments to experiments performed with the same laser and plasma density but using a guiding channel[10](see above), we find that the stability of the beam at high energy was greatly increased by the guiding channel, as expected from the analysis above. In the unchanneled case at a density of 2×10^{19} cm^{-3}, most shots produced no detectable charge at 80 MeV (detection threshold 10^7 electrons using the phosphor screen of the magnetic spectrometer), and fluctuation in charge was two orders of magnitude. In the channeled accelerator, by contrast, at the same density almost all

14

shots showed substantial charge at high energy and fluctuation was less than one order of magnitude. Charge at high energy was also at least two times higher. This is consistent with the mode image observations above, and indicates the advantage of channeled experiments. The plasma channel greatly improves the intensity and reproducibility of the output optical mode image, which measures how effectively the drive pulse focus (and hence plasma wave amplitude) was retained through the plasma. Remaining fluctuation in the channeled case appears to result primarily from pointing jitter of the laser spot into the channel, and it should therefore be possible to reduce this fluctuation further with stabilization.

Consistent with the explanation presented here, monoenergetic beams have also been observed in experiments at other laborotories using a large laser spot size to increase Z_R and hence the propagation distance of the laser pulse[11,12]. Like the unchanneled experiments described above, this method is less efficient than use of a plasma channel in terms of amount of charge accelerated and electron bunch energy per laser power because large spot size is required to obtain long the Z_R required. This reduces laser intensity, and hence wake amplitude and trapping.

Quality of the beams is also influenced by the reliance on beam loading to turn off injection at the appropriate time. This introduces a sensitive dependence on laser power and energy as well as plasma density. In the PIC simulations, variations as little as 10 % in laser energy were sufficient to change or broaden the electron distribution. In the experiments, laser power and energy typically fluctuated by approximately 10 %, and we observed fluctuation between continuous and structured energy spectra shot-to-shot, consistent with this explanation. Improvements in laser stability as well as controlled electron injection[17–21] offer a path to stabilized electron bunches of even higher quality.

V. CONCLUSIONS

In conclusion, experiments at the L'OASIS facility of LBNL with channeled and unchanneled self modulated wakefield accelerators have demonstrated that it is possible to produce structured energy spectra with significant fractions of the total charge in bunches with few MeV energy spread. Simulations and experiments varying target density and length indicate that the high quality beams are obtained by taking advantage of beam loading to produce a self-consistent phased injection of the electrons, and by matching the acceleration length

to the length over which the electrons dephase from the wake to reduce energy spread. At high densities this can be done using a very short gas jet, but this leads to low peak energies and low efficiency. At lower density, longer acceleration distances and higher peak energies are obtained. The long acceleration distance at low densities requires maintaining the intensity of the drive laser over mm scales, and channeled experiments then demonstrate clear advantage in beam charge, quality, and stability.

The beams from channel guided accelerators such as those described here open up a new class of experiments with laser accelerators. Improvements in laser stability as well as controlled electron injection will help to further stabilize and improve the properties of the electron bunches. Production of radioisotopes can immediately benefit from the higher average charge at high energy[52]. Beams with high spectral density at high energy will enable more efficient use of these accelerators as radiation sources for physics, chemistry and biology[13,15]. The bright and intrinsically ultrafast nature of the beams in particular will enable probing of time resolved phenomena with unprecedented resolution. As issues of stability and reproducibility are addressed, these beams may be of suitable quality to serve as injectors for high energy physics applications. Due to their good emittance, these beams also may offer focusability and luminosity competitive with state of the art rf accelerators. Such beams may be injected into and post accelerated in subsequent laser accelerator stages to produce compact multi stage electron linacs.

* Paper HI2 2, Bull. Am. Phys. Soc. **49**, 176 (2004)

† Also at University of California, Berkeley; Invited speaker; Electronic address: `cgrgeddes@lbl.gov`

‡ Also at Technische Universiteit Eindhoven, the Netherlands

§ Also at University of Colorado, Boulder

¶ URL: `http://loasis.lbl.gov`

[1] A. Modena, Z. Najmudin, A. E. Dangor, C. E. Clayton, K. A. Marsh, C. Joshi, V. Malka, C. B. Darrow, C. Danson, D. Neely, et al., Nature **377**, 606 (1995).

[2] K. Nakajima, D. Fisher, T. Kawakubo, H. Nakanishi, A. Ogata, Y. Kato, Y. Kitagawa, R. Kodama, K. Mima, H. Shiraga, et al., Phys. Rev. Lett. **74**, 4428 (1995).

[3] D. Umstadter, S.-Y. Chen, A. Maksimchuk, G. Mourou, and R. Wagner, Science **273**, 472 (1996).

[4] C. Moore, A. Ting, K. Krushelnick, E. Esarey, R. F. Hubbard, H. R. Burris, C. Manka, and P. Sprangle, Phys. Rev. Lett. **79**, 3909 (1997).

[5] D. Gordon, K. C. Tzeng, C. E. Clayton, A. E. Dangor, V. Malka, K. A. Marsh, A. Modena, W. B. Mori, P. Muggli, Z. Najmudin, et al., Phys. Rev. Lett. **80**, 2133 (1998).

[6] V. Malka, S. Fritzler, E. Lefebvre, M. M. Aleonard, F. Burgy, J. P. Chambaret, J. F. Chemin, K. Krushelnick, G. Malka, S. P. D. Mangles, et al., Science **298**, 1596 (2002).

[7] W. P. Leemans, P. Catravas, E. Esarey, C. G. R. Geddes, C. Toth, R. Trines, C. B. Schroeder, B. A. Shadwick, J. van Tilborg, and J. Faure, Phys. Rev. Lett. **89**, 4802 (2002).

[8] T. Tajima and J. M. Dawson, Phys. Rev. Lett. **43**, 267 (1979).

[9] E. Esarey, P. Sprangle, J. Krall, and A. Ting, IEEE Trans. Plasma Sci. **24**, 252 (1996).

[10] C. G. R. Geddes, C. Toth, J. van Tilborg, E. Esarey, C. B. Schroeder, D. Bruhwiler, C. Nieter, J. Cary, and W. P. Leemans, Nature **431**, 538 (2004).

[11] J. Faure, Y. Glinec, A. Pukhov, S. Kiselev, S. Gordienko, E. Lefebvre, J.-P. Rousseau, F. Burgy, and V. Malka, Nature **431**, 541 (2004).

[12] S. P. D. Mangles, C. D. Murphy, Z. Najmudin, A. G. R. Thomas, J. L. Collier, A. E. Dangor, E. J. Divall, P. S. Foster, J. G. Gallacher, C. J. Hooker, et al., Nature **431**, 535 (2004).

[13] P. Catravas, E. Esarey, and W. P. Leemans, Meas. Sci. Tech. **12**, 1828 (2001).

[14] R. W. Schoenlein, W. P. Leemans, A. H. Chin, P. Volfbeyn, T. E. Glover, P. Balling, M. Zolo-torev, K. J. Kim, S. Chattopadhyay, and C. V. Shank, Science **274**, 236 (1996).

[15] W. P. Leemans, C. G. R. Geddes, J. Faure, C. Toth, J. van Tilborg, C. B. Schroeder, E. Esarey, G. Fubiani, D. Auerbach, B. Marcelis, et al., Phys. Rev. Lett. **91**, 4802 (2003).

[16] X. J. Wang, X. Qiu, and I. Ben-Zvi, Phys. Rev. E **54**, R3121 (1996).

[17] D. Umstadter, J. K. Kim, and E. Dodd, Phys. Rev. Lett. **76**, 2073 (1996).

[18] E. Esarey, R. F. Hubbard, W. P. Leemans, A. Ting, and P. Sprangle, Phys. Rev. Lett. **79**, 2682 (1997).

[19] C. B. Schroeder, P. B. Lee, J. S. Wurtele, E. Esarey, and W. P. Leemans, Phys. Rev. E **59**, 6037 (1999).

[20] G. Fubiani, E. Esarey, C. B. Schroeder, and W. P. Leemans, Physical Review E **70**, 016402 (2004).

[21] C. Moore, A. Ting, S. McNaught, J. Qiu, H. Burris, and P. Sprangle, Phys. Rev. Lett. **82**, 1688 (1999).

[22] J. Krall, A. Ting, E. Esarey, and P. Sprangle, Phys. Rev. E **48**, 2157 (1993).

[23] C. Nieter and J. Cary, J. Comp. Phys. **196**, 448 (2004).

[24] P. Volfbeyn, E. Esarey, and W. P. Leemans, Phys. Plasmas **6**, 2269 (1999).

[25] W. P. Leemans, P. Volfbeyn, K. Z. Guo, S. Chattopadhyay, C. B. Schroeder, B. A. Shadwick, P. B. Lee, J. S. Wurtele, and E. Esarey, Phys. Plasmas **5**, 1615 (1998).

[26] C. Toth, J. van Tilborg, C. R. Geddes, G. Fubiani, C. B. Schroeder, E. Esarey, J. Faure, G. Dugan, and W. P. Leemans, in *High Power Laser Ablation V, Taos NM* (SPIE, Bellingham WA, 2004).

[27] D. Strickland and G. Mourou, Opt. Comm. **56**, 219 (1985).

[28] W. P. Leemans, C. E. Clayton, W. B. Mori, K. A. Marsh, P. K. Kaw, A. Dyson, C. Joshi, and J. M. Wallace, Phys. Rev. A **46**, 1091 (1992).

[29] R. Rankin, C. E. Capjack, and N. H. B. an P. B. Corkum, Opt. Lett. **16**, 835 (1991).

[30] H. M. Milchberg, T. R. Clark, C. G. Durfee III, and T. M. Antonsen, Phys. Plasmas **3**, 2149 (1996).

[31] C. G. Durfee III and H. M. Milchberg, Phys. Rev. Lett. **71**, 2409 (1993).

[32] K. Kim, I. Alexeev, J. Fan, E. Parra, and H. Milchberg, in *Advanced Accelerator Workshop, Mandalay bay 2002* (AIP, New York, 2002), p. 646.

[33] E. W. Gaul, S. P. Le Blanc, A. R. Rundquist, R. Zgadzaj, H. Langhoff, and M. C. Downer, Appl. Phys. Lett. **77**, 4112 (2000).

[34] Y. Ehrlich, C. Cohen, A. Zigler, J. Krall, P. Sprangle, and E. Esarey, Phys. Rev. Lett. **77**, 4186 (1996).

[35] E. Esarey, P. Sprangle, J. Krall, and A. Ting, IEEE J. Quantum Electron. **33**, 1879 (1997).

[36] A. Litvak, Sov. Phys JETP **30**, 344 (1969).

[37] P. Sprangle, C. M. Tang, and E. Esarey, IEEE Trans. Plasma Sci. **PS-15**, 145 (1987).

[38] E. Esarey, J. Krall, and P. Sprangle, Phys. Rev. Lett. **72**, 2887 (1994).

[39] W. B. Mori, IEEE J. Quantum Electron. **33**, 1942 (1997).

[40] Z. Najmudin, K. Krushelnick, E. Clark, S. Mangles, B. Walton, A. Dangor, S. Fritzler, V. Malka, E. Lefebvre, D. Gordon, et al., Phys. Plasmas **10**, 2071 (2003).

[41] A. B. Borisov, A. V. Borovskiy, O. B. Shiryaev, V. V. Korobkin, A. M. Prokhorov, J. C. Solem, T. S. Luk, K. Boyer, and C. K. Rhodes, Phys. Rev. A **45**, 5830 (1992).

[42] C. G. R. Geddes, C. Toth, J. van Tilborg, E. Esarey, C. B. Schroeder, D. Bruhwiler, C. Nieter, J. Cary, and W. P. Leemans, Submitted to Phys. Rev. Lett. (2004).

[43] R. F. Hubbard, D. Kaganovich, B. Hafizi, C. I. Moore, P. Sprangle, A. Ting, and A. Zigler, Phys. Rev. E **63**, 036502 (2001).

[44] T. Katsouleas, S. Wilks, P. Chen, J. M. Dawson, and J. J. Su, Part. Accel. **22**, 81 (1987).

[45] F. Tsung and W.B. Mori, private communication, 2004.

[46] S. V. Bulanov, F. Pegoraro, A. M. Pukhov, and A. S. Sakharov, Phys. Rev. Lett. **78**, 4205 (1997).

[47] C. B. Schroeder, E. Esarey, B. A. Shadwick, and W. P. Leemans, in *Advanced Accelerator Concepts*, edited by V. Yakimenko (AIP, New York, 2004), pp. 564–570.

[48] F. S. Tsung, R. Narang, W. B. Mori, C. Joshi, R. A. Fonseca, and L. O. Silva, Phys. Rev. Lett. **93** (2004).

[49] A. J. W. Reitsma, W. P. Leemans, E. Esarey, C. B. Schroeder, L. P. J. Kamp, and T. J. Schep, Phys. Rev. ST Accel. Beams **5**, 051301 (2002).

[50] A. Pukhov and J. Meyer-ter-Vehn, Appl. Phys. B **74**, 355 (2002).

[51] E. Esarey and M. Pilloff, Phys. Plasmas **2**, 1432 (1995).

[52] W. P. Leemans, D. Rodgers, P. E. Catravas, C. G. R. Geddes, G. Fubiani, E. Esarey, B. A. Shadwick, R. Donahue, and A. Smith, Phys. Plasmas **8**, 2510 (2001).

FIG. 1: Schematic of the channel guided wakefield accelerator, showing laser beams and principal diagnostics. A plasma is formed by an ignitor laser pulse in a pulsed hydrogen gas jet and heated by a heater pulse. A high intensity drive pulse is focused at the edge of the resulting plasma channel, in which it drives a plasma wave, accelerating electrons. Propagation of the laser is monitored with a side interferometer and mode imager CCD. The electron beam is analyzed using an integrating current transformer (ICT), a phosphor screen, and a magnetic spectrometer.

FIG. 2: Plasma channel formed by the ignitor and heater pulses at the time of arrival of the drive pulse. A frequency doubled interferometer images the plasma transversely (A). The transverse density profile (B) was obtained from Abel inversion of the resulting phase map with cylindrical symmetry about the z axis, showing data (black dots) and a parabolic fit (red line).

FIG. 3: Propagation of the laser through the gas jet was measured by the side looking interferometer (A,C) and mode (laser spot) imager (B,D). In the channel guided accelerator, the plasma interferogram after the passage of the drive beam (A) was similar to the guiding channel (see Fig. 2A), indicating that the drive laser pulse is confined to the channel. The laser mode at the channel exit is a well defined spot of $24\mu m$ FWHM after 2.4 mm of propagation (B). When the channel is off, the interferogram (C) shows a plasma expanding rapidly along the propagation direction (left to right). The mode image (D) shows a diffuse transmitted spot. This indicates the effectiveness of the channel in maintaining the drive beam intensity and mode over many diffraction lengths.

FIG. 4: Single shot electron beam spectrum of the channel guided accelerator, showing a strongly peaked distribution, in contrast to the exponential distribution of the unchanneled accelerator. A contour plot of electron beam intensity versus energy and divergence shows a bunch containing 2×10^9 electrons in a narrow distribution at 86 ± 1.8 MeV and 3 mrad divergence FWHM with contrast$> 10 : 1$ above background.

FIG. 5: Profile of the electron beam, showing the spatial distribution 72 cm after exiting the plasma. The profile was measured using a phosphor screen placed in the beam, imaged by a CCD camera. The channel guided accelerator (A) produces collimated beams with divergence near 6 mrad FWHM. The unchanneled accelerator produced diffuse electron beams with a much wider divergence of 50 mrad FWHM (B).

FIG. 6: Normalized electron charge above 100 MeV versus guided mode intensity. Data are binned from 300 shots, and normalized to the highest values observed during the run. High energy beams are highly correlated with high guided mode intensities, indicating that maintaining the drive laser intensity over the length of the plasma using the channel enhances accelerator performance.

FIG. 7: Simulation momentum phase space (top of each panel) and laser envelope (bottom) as a function of propagation distance, $x[\mu m]$. The laser enters the plasma (A), and is modulated by the plasma response, exciting a wake and trapping electrons (B). If trapping turns off after the initial bunch is loaded (see Fig. 8), these electrons are concentrated in energy at the dephasing length, forming a high energy low energy spread bunch (C) which dissipates with further propagation (D).

FIG. 8: Simulated electron density after laser propagation of 875 μm (A) and 1117 μm (B), showing the wake and the effect of the trapped electrons on it. Just before trapping in the first bucket behind the laser (A), the wake structure is undisturbed and large in amplitude, allowing self trapping of electrons. When a bunch is trapped, the wake is damped, suppressing further trapping and hence isolating the initial bunch in phase space (B). The bunch is visible in (B) as a small isolated dot in the center of the first bucket, with density comparable to the plasma density. Buckets further behind the pulse trap and dephase earlier; accordingly, bunches are visible in trailing buckets before trapping in the first.

21

FIG. 9: Electron energy spectrum for the unchanneled accelerator operated at a density of 4×10^{19} cm^{-3}, obtained by scanning the magnet current over many shots. For a plasma length of 600 μm, near the dephasing length calculated in simulations, there is several times more charge at high energy than for a 1.8 mm long plasma, which is longer than the dephasing length. The insets show individual phosphor images, demonstrating that the spectrum is also more structured at the dephasing length, consistent with simulation. Fluctuation in the spectrum appears due to fluctuations in self-guiding and in laser parameters shot-to-shot.

FIG. 10: Electron energy spectrum for the unchanneled accelerator operated at a density of 2×10^{19}cm^{-3}, obtained by scanning the magnet current over many shots. For a plasma length of 600 μm, before the dephasing length calculated in simulations, very low energies are produced compared to a 4 mm plasma, which is longer than the dephasing length. The insets show individual phosphor images, demonstrating that the spectrum is also unstructured and smooth before the dephasing point, consistent with the explanation that particles are bunched in energy at dephasing. Fluctuation in the spectrum appears due to fluctuations in self-guiding and in laser parameters shot-to-shot.

Drive pulse
500mJ 55fs

Heater pulse
150mJ 250ps

2ω
probe

Gas jet

Phosphor

Ignitor pulse
15mJ 60fs

e⁻

ICT

Interferometer

Mode
Imager

Magnet

Figure 1

410
r,μm

0   z,μm   4200
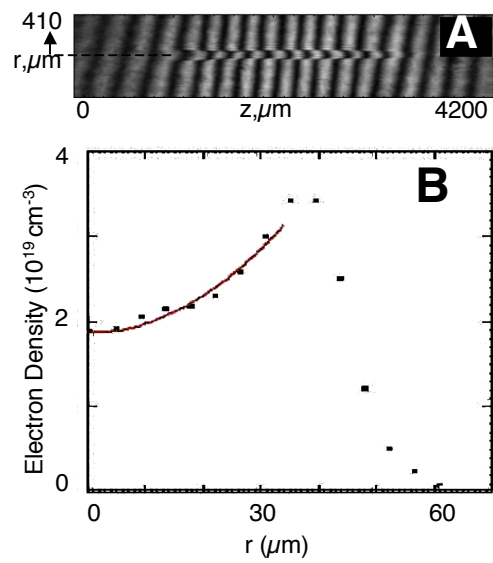
A

4

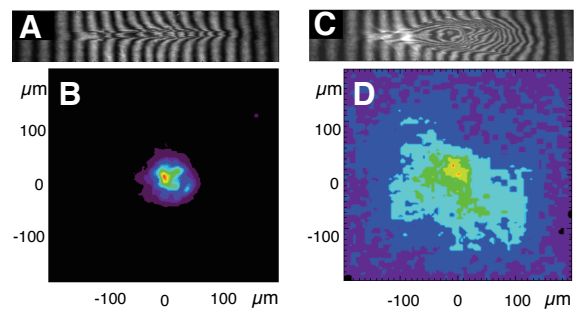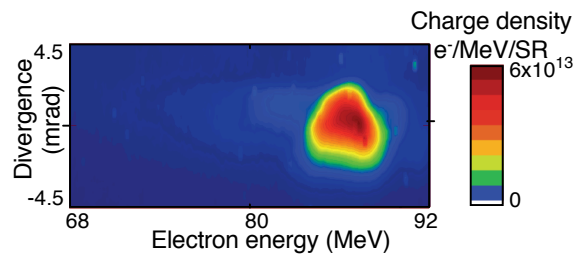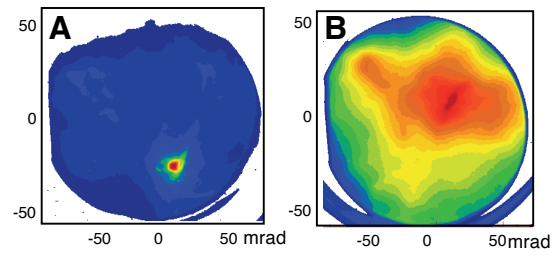Electron Density (10^{19} cm^{-3})

B

2
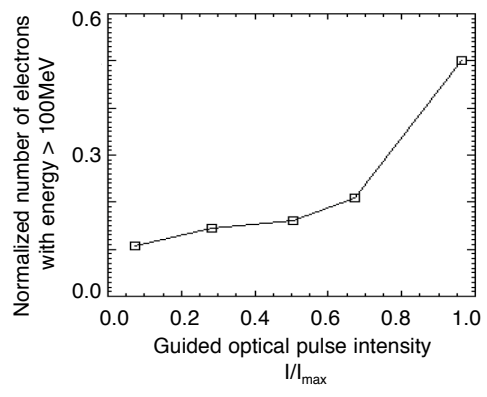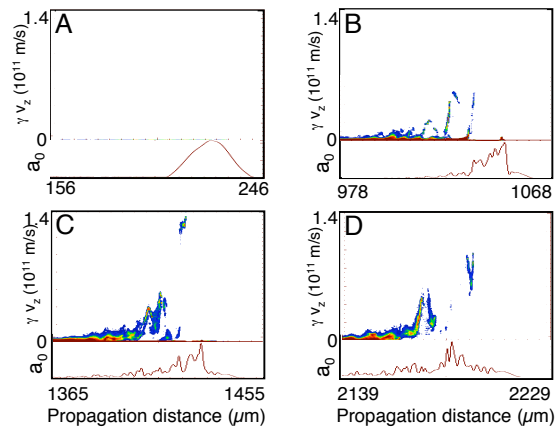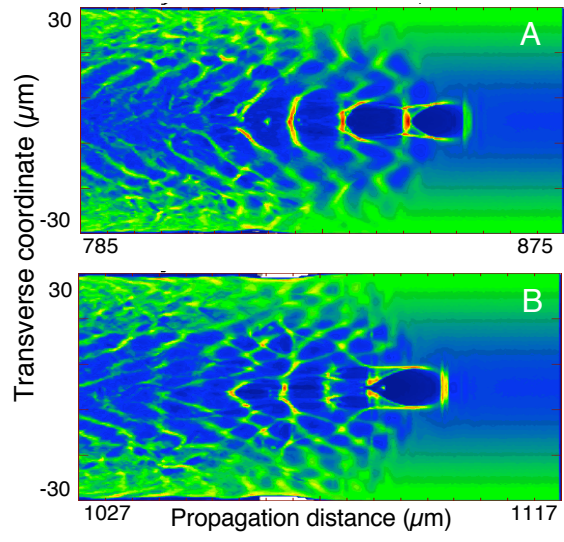
0

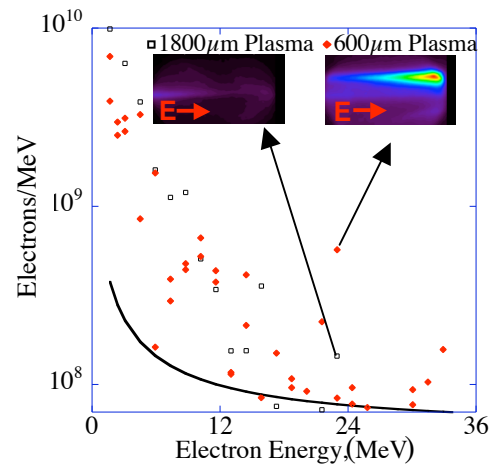0   30   60
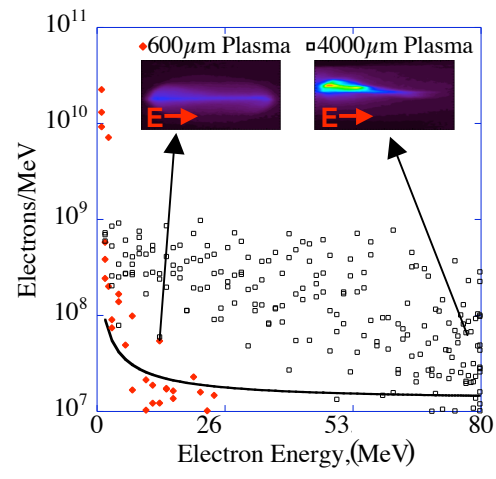
r (μm)
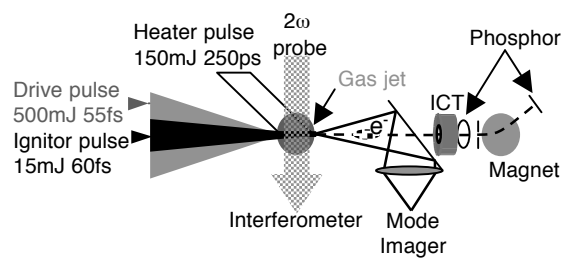
Figure 2

Figure 3

Figure 4

Figure 5

Figure 6

Figure 7

Figure 8

Figure 9

Figure 10